ELSEVIER

Physica D 132 (1999) 339–362

PHYSICA D

www.elsevier.com/locate/physd

Pattern formation in three-dimensional reaction–diffusion systems

T.K. Callahan [a,b], E. Knobloch [a,*]

[a] *Department of Physics, University of California, Berkeley, CA 94720, USA*
[b] *Department of Mathematics, University of Michigan at Ann Arbor, Ann Arbor, MI 48109, USA*

Received 17 August 1998; received in revised form 1 February 1999; accepted 9 February 1999
Communicated by J.D. Meiss

Abstract

Existing group theoretic analysis of pattern formation in three dimensions [T.K. Callahan, E. Knobloch, Symmetry-breaking bifurcations on cubic lattices, Nonlinearity 10 (1997) 1179–1216] is used to make specific predictions about the formation of three-dimensional patterns in two models of the Turing instability, the Brusselator model and the Lengyel–Epstein model. Spatially periodic patterns having the periodicity of the simple cubic (SC), face-centered cubic (FCC) or body-centered cubic (BCC) lattices are considered. An efficient center manifold reduction is described and used to identify parameter regimes permitting stable lamellæ, SC, FCC, double-diamond, hexagonal prism, BCC and BCCI states. Both models possess a special wavenumber k_* at which the normal form coefficients take on fixed model-independent ratios and both are described by identical bifurcation diagrams. This property is generic for two-species chemical reaction–diffusion models with a single activator and inhibitor.

PACS: 82.40.Bj; 47.54.+r; 47.20.Ky; 87.10.+e

Keywords: Turing instability; Brusselator and Lengyel–Epstein models; Three-dimensional patterns

1. Introduction

The instability now identified with Alan Turing's name [1] is believed to be involved in the formation of structure in many systems of biological interest [2]. The instability leads to a process that might be called differentiation and in its simplest realization is the result of a competition between an activator and an inhibitor diffusing at different rates. The instability that results has one characteristic property: its scale or wavelength is determined by the concentrations of ambient species and the diffusion coefficients, and is therefore independent of any externally imposed length scales. In the process of morphogenesis the instability is likely to be triggered by the increasing scale of the system: the instability occurs once the system is large enough that it contains several natural wavelengths of the instability.

* Corresponding author. Fax: +1-510-643-8497; e-mail: knobloch@physics.berkeley.edu.

0167-2789/99/$ – see front matter
PII: S0167-2789(99)00041-X

The formation of structure or 'patterns' by the Turing instability has been investigated in a number of models of the instability. One of the most popular of these is the Brusselator model [3]. These studies include the formation of structure in one dimension, either with periodic boundary conditions designed to mimic large systems [4], or with mixed boundary conditions appropriate for realistic finite systems [5]. In one dimension the former subsume the case of no-flux (or Neumann) boundary conditions. Similar studies have also been carried out in two [6] and three dimensions [7–9], usually with periodic boundary conditions. In the plane the general theory describing the spatially periodic patterns arising from a spontaneous symmetry-breaking steady state instability in isotropic homogeneous systems is described in [10] (see also [11]). The theory focuses on patterns symmetric with respect to the symmetry operations preserving a particular two-dimensional lattice, for example, the square or the hexagonal lattice generated by wavevectors of magnitude k_T, where $2\pi/k_T$ is the instability wavelength. This assumption selects four (resp., six) wavevectors from the circle of marginally stable wavevectors present at onset. The theory then uses group-theoretic techniques to construct coupled evolution equations for the evolution of the amplitudes of these wavevectors. These equations predict the basic sequence of transitions that may be expected as a bifurcation parameter is varied. For applications to specific models of the instability it is necessary to compute the coefficients in these equations from the partial differential equations of the model with periodic boundary conditions. This is typically done using center manifold reduction. Because of the use of periodic boundary conditions with period $2\pi/k_T$ the aspect ratio of the system is not a parameter of the problem, although effects of *forced* breaking of translation invariance (due to distant sidewalls) can be included by other methods [12]. Instead the theory uses one of the externally imposed concentrations as the bifurcation parameter. The predictions of the resulting theory agree well with the results of numerical integration of the model partial differential equations [6], at least for the Brusselator model. Other lattices, with larger basic cell relative to the wavelength, can also be used, and allow the study of more complex patterns [13].

Because of its intrinsic wavelength the Turing instability readily forms three-dimensional structures as well. In sufficiently large domains such structures can be essentially periodic. It makes sense, therefore, to extend the type of theory summarized above to three dimensions. For states with cubic symmetry, such an extension was recently completed [14], and allows us to make systematic predictions of the types and stability properties of three-dimensional patterns that arise in various models of the Turing instability. The purpose of the present paper is to make such predictions for two models, the Brusselator model already mentioned, and the more recent Lengyel–Epstein model [15]. In Section 2 we summarize the predictions of the theory for three lattices with cubic symmetry: the simple cubic (SC), the face-centered cubic (FCC) and the body-centered cubic (BCC). In each case we simply list the relevant amplitude equations together with the types of patterns that form in the primary symmetry-breaking instability. We do not derive these equations here, nor do we discuss abstractly their stability properties. For these the reader is referred to the paper by Callahan and Knobloch [14]. We truncate the amplitude equations at third order in the pattern amplitude, and use these to introduce the coefficients that have to be computed from the two models. The results of the center manifold reduction used to evaluate these coefficients are summarized in Sections 3 and 4 while the details of the reduction procedure are relegated to Appendix A. These sections also refer to the existing theory for the construction of the resulting bifurcation diagrams. In both models the coefficients can be expressed in terms of a single dimensionless parameter we call R. This fact allows us to divide the space of coefficients into regions with different diagrams, and indicate the trajectory through this space as R is varied, i.e., how one bifurcation diagram changes into the next one. We find that on the simple cubic lattice a one-dimensional state we call lamellæ can be stable, as can the three-dimensional simple cubic state, and identify the ranges in R where these states are expected. Similarly, on the face-centered cubic lattice we show that both lamellæ and the two three-dimensional states we call FCC and double-diamond states can be stable, while on the BCC lattice we find that generically there are no stable patterns near onset. In this case we show, by examining the regime in which the coefficient of the quadratic terms in the amplitude equations is small, that a number of these unstable branches acquire stability at

secondary bifurcations, and show that as a result two three-dimensional states we call BCC and BCCI can become stable. Hexagonal prisms and lamellæ can also acquire stability at finite amplitude. In Section 5 we compare the predictions for the two models and summarize their implications. Although we do not carry out simulations of the model partial differential equations we do compare our results with the three-dimensional simulations of the Brusselator reported in [8,9].

We use two models, the first of which is the Brusselator [3],

$$\dot{X} = -(B+1)X + X^2Y + A + D_x\nabla^2 X, \qquad \dot{Y} = BX - X^2Y + D_y\nabla^2 Y. \tag{1}$$

Here X and Y are the chemical concentrations of an activator and an inhibitor, respectively, D_x and D_y are their diffusivities ($D_x < D_y$), and A and B are parameters which are held fixed. Although the Brusselator has been much studied as a model system exhibiting a Turing instability it is not a model for any specific chemical system per se. In contrast the second system we study, the Lengyel–Epstein model [15], models the chlorite–iodide–malonic acid (CIMA) reaction in which the Turing instability was first experimentally established [16]. More precisely, the Lengyel–Epstein model describes the closely related chlorine dioxide–iodine–malonic acid (CDIMA) reaction which also exhibits the Turing instability. Like the Brusselator the Lengyel–Epstein model is a two species model with one equation for an activator (I^-) and another for an inhibitor (ClO_2^-). In dimensionless variables the model takes the form

$$\dot{X} = a - X - \frac{4XY}{1+X^2} + \nabla^2 X, \qquad \dot{Y} = \delta\left[b\left(X - \frac{XY}{1+X^2}\right) + c\nabla^2 Y\right], \tag{2}$$

where X and Y again represent the activator and inhibitor concentrations, c is the ratio of their diffusivities, and a and b are fixed parameters. In aqueous solution c is generally close to one and consequently the conditions for the Turing instability are not satisfied. However, if starch is present, the iodide mobility is dramatically reduced (because of the binding of I^- to the starch) and the effective diffusivity ratio becomes larger by the factor $\delta > 1$. Thus the starch plays a vital if passive role in the appearance of the instability. A detailed derivation of the model and its confrontation with experiments is described in [17].

Both models require four parameters for their complete specification. We think of two of these, A and B (resp., a, b), as representing concentrations of input chemicals, while the remaining two specify the diffusion rates of the activator and inhibitor. Moreover, the nonlinear terms in the activator and inhibitor equations are of the same form in each model. This fact, as we shall see, has important consequences for the properties of these models. In the following we first describe the general theory we use to study pattern formation in three dimensions; this theory is completely model-independent but depends on certain coefficients which are model-specific. Thus the application of the theory to these two models reduces to the computation of these coefficients.

2. Amplitude equations for three-dimensional patterns

In this section we describe the construction of the amplitude equations governing the evolution of three-dimensional spatially periodic patterns. The discussion is in terms of a bifurcation parameter B that occurs in the Brusselator model (1) but is otherwise completely general. We consider a system of reaction–diffusion equations with a spatially uniform equilibrium state and suppose that as B varies this equilibrium state loses stability to an exponentially growing perturbation of *finite* wavenumber k_T when B reaches a critical value B_T (see Fig. 1). In the following we focus on spatially *periodic* patterns only, and consequently formulate the resulting bifurcation problem on a three-dimensional lattice. Such a lattice is invariant under translations in three independent directions and the symmetries of the unit cell. This assumption is equivalent to the selection of a *finite* set of $2N$ wavevectors from

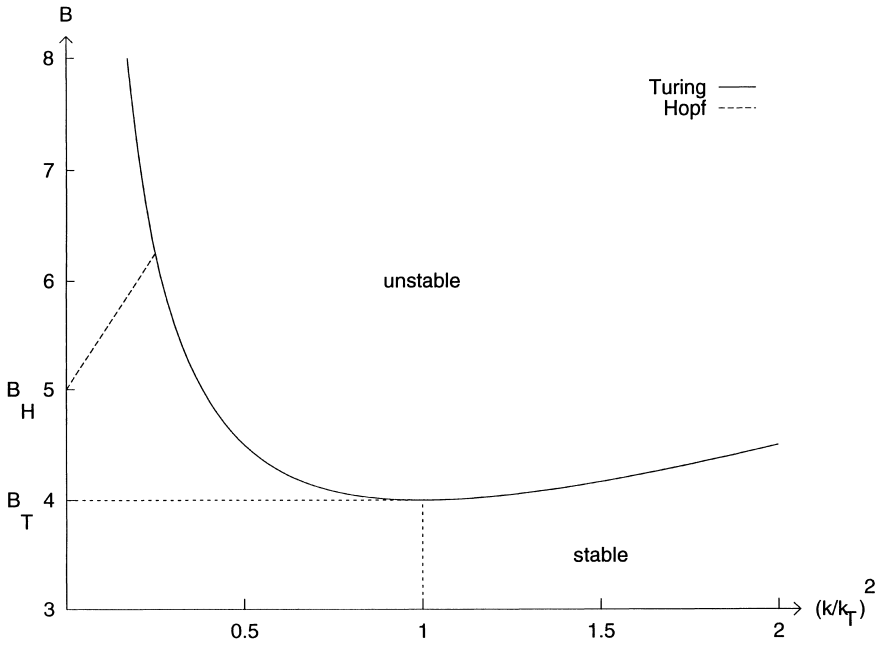

Fig. 1. The neutral stability curve $B(k)$ for the Brusselator model with $A = 2$ and $D_y = 4D_x$.

the sphere of marginally stable wavevectors present at $B = B_{\mathrm{T}}$. In the following we assume that the unit cell is generated by wavevectors of length k_{T} and that it has *cubic* symmetry. There are three fundamental possibilities for choosing such wavevectors and these lead to the SC lattice, the FCC lattice and the BCC lattice. In each of these cases the partial differential equations can be projected onto the corresponding Fourier modes and the resulting infinite-dimensional set of ordinary differential equations reduced, via *center manifold reduction* [18], to a finite set of ordinary differential equations for the $2N$ near-marginal modes valid near $B = B_{\mathrm{T}}$. In terms of these modes the concentration $X(\boldsymbol{x})$ is given by

$$X(\boldsymbol{x}) = \sum_{j=1}^{2N} z_j \, e^{\mathrm{i}\boldsymbol{k}_j \cdot \boldsymbol{x}} + \text{n.l.t.},$$

where the $\boldsymbol{k}_j$ are the marginally stable wavevectors of length k_{T} and the z_j are their complex amplitudes. The terms denoted n.l.t. are *nonlinear* in the z_j and include the various harmonics of the $\boldsymbol{k}_j$ generated by the nonlinearities. This reduction procedure is described in detail for the Brusselator in Appendix A.

For the SC lattice, $N = 3$ and the critical wavevectors may be chosen to be

$$\boldsymbol{k}_1 = -\boldsymbol{k}_4 = k_{\mathrm{T}}(1, 0, 0), \qquad \boldsymbol{k}_2 = -\boldsymbol{k}_5 = k_{\mathrm{T}}(0, 1, 0), \qquad \boldsymbol{k}_3 = -\boldsymbol{k}_6 = k_{\mathrm{T}}(0, 0, 1),$$

relative to Cartesian coordinates (x, y, z). For systems with the periodicity of the FCC lattice, $N = 4$ and the critical wavevectors are

$$\boldsymbol{k}_1 = -\boldsymbol{k}_5 = \frac{k_{\mathrm{T}}}{\sqrt{3}}(1, 1, 1), \qquad \boldsymbol{k}_2 = -\boldsymbol{k}_6 = \frac{k_{\mathrm{T}}}{\sqrt{3}}(1, -1, -1), \qquad \boldsymbol{k}_3 = -\boldsymbol{k}_7 = \frac{k_{\mathrm{T}}}{\sqrt{3}}(-1, 1, -1),$$
$$\boldsymbol{k}_4 = -\boldsymbol{k}_8 = \frac{k_{\mathrm{T}}}{\sqrt{3}}(-1, -1, 1).$$

Finally, for the BCC lattice, $N = 6$ and the critical wavevectors are

$$\boldsymbol{k}_1 = -\boldsymbol{k}_7 = \frac{k_\mathrm{T}}{\sqrt{2}}(1,1,0), \qquad \boldsymbol{k}_2 = -\boldsymbol{k}_8 = \frac{k_\mathrm{T}}{\sqrt{2}}(0,1,1), \qquad \boldsymbol{k}_3 = -\boldsymbol{k}_9 = \frac{k_\mathrm{T}}{\sqrt{2}}(1,0,1),$$
$$\boldsymbol{k}_4 = -\boldsymbol{k}_{10} = \frac{k_\mathrm{T}}{\sqrt{2}}(1,-1,0), \qquad \boldsymbol{k}_5 = -\boldsymbol{k}_{11} = \frac{k_\mathrm{T}}{\sqrt{2}}(0,1,-1), \qquad \boldsymbol{k}_6 = -\boldsymbol{k}_{12} = \frac{k_\mathrm{T}}{\sqrt{2}}(-1,0,1).$$

Since X is a real scalar the amplitudes of equal and opposite wavevectors must be complex conjugates of one another. Thus the SC case is described by three coupled equations of the form

$$\frac{\mathrm{d}}{\mathrm{d}t}\begin{pmatrix} z_1 \\ z_2 \\ z_3 \end{pmatrix} = \begin{pmatrix} f_1(z_1,z_2,z_3) \\ f_2(z_1,z_2,z_3) \\ f_3(z_1,z_2,z_3) \end{pmatrix},$$

while the FCC and BCC cases are described by four- and six-dimensional systems. The structure of these equations follows from the equivariance condition

$$\gamma \cdot \boldsymbol{f}(\boldsymbol{z}) = \boldsymbol{f}(\gamma \cdot \boldsymbol{z}), \quad \forall \gamma \in \Gamma, \tag{3}$$

expressing the requirement that if $\boldsymbol{z}$ is a state of the system, so is $\gamma \cdot \boldsymbol{z}$. Here Γ is the symmetry group of the lattice on which the problem is defined, i.e., the group $\Gamma = T^3 \dot{+} \boldsymbol{O} \oplus \boldsymbol{Z}_2$. Here T^3 is the three-torus of translations, $\boldsymbol{O}$ is the group of orientation-preserving symmetries of the cube, and the non-trivial element of $\boldsymbol{Z}_2$ represents inversion through the origin. The three-torus T^3 acts upon each amplitude by

$$\hat{a} : z_j \to z_j \, \mathrm{e}^{\mathrm{i}\boldsymbol{k}_j \cdot \boldsymbol{a}}, \quad \boldsymbol{a} \in \boldsymbol{R}^3.$$

while $\hat{c} \in \boldsymbol{Z}_2$ acts by

$$\hat{c} : z_j \to \bar{z}_j.$$

The group $\boldsymbol{O}$ acts differently upon each of the lattices, but in each case is a group of permutations of the z_j. The form of the resulting equations is independent of the specific model under consideration. Consequently, the reduced equations can be studied abstractly first, as done in [14], to determine the number of possible solutions and their stability properties.

The equivariance condition (3) determines the form of $\boldsymbol{f}$. To third order in the amplitudes z_j the most general possible system for the SC lattice is

$$\dot{z}_1 = \lambda z_1 + h_{1,\sigma_1}(|z_1|^2 + |z_2|^2 + |z_3|^2)z_1 + h_3|z_1|^2 z_1, \tag{4}$$

where h_{1,σ_1} and h_3 are real coefficients and $\lambda \propto (B - B_\mathrm{T})$. To this equation one must append equations for $\dot{z}_2$ and $\dot{z}_3$ obtained by applying appropriate elements $\gamma \in \Gamma$ to Eq. (4). Thus $f_2(z_1,z_2,z_3) = f_1(z_2,z_1,z_3)$ and $f_3(z_1,z_2,z_3) = f_1(z_3,z_2,z_1)$. For the FCC lattice the corresponding system is

$$\dot{z}_1 = \lambda z_1 + h_{1,\sigma_1}(|z_1|^2 + |z_2|^2 + |z_3|^2 + |z_4|^2)z_1 + h_3|z_1|^2 z_1 + p_3 \bar{z}_2 \bar{z}_3 \bar{z}_4, \tag{5}$$

while for the BCC lattice, the system is

$$\begin{aligned}\dot{z}_1 = {} & \lambda z_1 + \tfrac{1}{2}a_{12}(z_2\bar{z}_6 + z_3 z_5) + a_1|z_1|^2 z_1 + \tfrac{1}{4}a_3(|z_2|^2 + |z_3|^2 + |z_5|^2 + |z_6|^2)z_1 + a_8|z_4|^2 z_1 \\ & + \tfrac{1}{2}a_{16}(z_2 z_4 z_5 + z_3 \bar{z}_4 z_6).\end{aligned} \tag{6}$$

Again, the remaining equations are generated by applying suitable $\gamma \in \Gamma$ to Eqs. (5) and (6). Note that, in contrast to the SC and FCC cases, the BCC equations contain a quadratic equivariant. The presence of this term has a

Table 1
Maximal isotropy branches for the SC lattice

Name	Solution	σ_1	Branching equation
Trivial	(0,0,0)	0	$\sigma_1 = 0$
Lamellæ	$(x, 0, 0)$	x^2	$\lambda + (h_{1,\sigma_1} + h_3)\sigma_1 = 0$
Square prisms	$(x, x, 0)$	$2x^2$	$\lambda + \frac{1}{2}(2h_{1,\sigma_1} + h_3)\sigma_1 = 0$
Simple cubic	(x, x, x)	$3x^2$	$\lambda + \frac{1}{3}(3h_{1,\sigma_1} + h_3)\sigma_1 = 0$

profound effect on the stability of the solutions: all solutions near the primary bifurcation at $\lambda = 0$ are *unstable* [10]. Since we are looking for stable solutions we consider in the following the special case in which the coefficient a_{12} is *small*. The analysis of the resulting degenerate bifurcation allows us to capture *secondary* bifurcations that can stabilize the unstable primary branches, much as in the two-dimensional problem on the hexagonal lattice [11]. Consequently, in the following we impose an additional reflection symmetry $\boldsymbol{Z}_2(-I)$ with the action $\kappa : \boldsymbol{z} \to -\boldsymbol{z}$, $\kappa \in \boldsymbol{Z}_2(-I)$. This symmetry forces all even terms in Eq. (6) to vanish; the secondary bifurcations appear when this symmetry is weakly broken [14]. This procedure is not arbitrary. We show in Sections 3 and 4 that realizable values of the physical parameters exist for which a_{12} is indeed small, so that our results have a well-defined regime of applicability.

The behavior of the resulting equations depends on the values of the coefficients and these in turn depend on the physical problem under consideration and through that on the physical parameters. However, using group-theoretic techniques it is possible to analyze the properties of these equations once and for all, as done in [14]. These techniques allow us to identify solutions that are always present. For each representation of the symmetry group Γ (SC, FCC or BCC) we classify the nontrivial solutions (patterns) by their symmetries. For any solution $\boldsymbol{z} = (z_1, \ldots, z_N)$, we define its *isotropy subgroup* $\Sigma(\boldsymbol{z})$ to be

$$\Sigma \equiv \{\gamma \in \Gamma : \gamma \cdot \boldsymbol{z} = \boldsymbol{z}\}.$$

For each isotropy subgroup there is a *fixed point subspace*

$$\mathrm{Fix}(\Sigma) \equiv \{\boldsymbol{z} \in \boldsymbol{C}^N : \sigma \cdot \boldsymbol{z} = \boldsymbol{z} \quad \forall \sigma \in \Sigma\}.$$

The usefulness of these definitions stems from the following [10]:

Equivariant Branching Lemma. *Let Γ be a Lie group acting absolutely irreducibly on $\boldsymbol{C}^N$ and let $\boldsymbol{f} \in \mathcal{E}_{\boldsymbol{z},\lambda}(\Gamma)$ be a Γ-equivariant bifurcation problem such that as λ passes through 0 a real eigenvalue of $(\mathrm{d}\boldsymbol{f})_{0,0}$ passes through the origin with non-zero speed. Let Σ be an isotropy subgroup satisfying*

$$\dim \mathrm{Fix}(\Sigma) = 1.$$

Then there exists a unique smooth solution branch to $\boldsymbol{f} = 0$ such that the isotropy subgroup of each solution is Σ.

A representation of a group Γ is *absolutely irreducible* if the only matrices which commute with all elements of Γ are multiples of the identity. This is true for all three representations of $\Gamma = T^3 \dot{+} \boldsymbol{O} \oplus \boldsymbol{Z}_2$ discussed in this paper.

For each of the lattices, the primary branches guaranteed by the Equivariant Branching Lemma are listed in Tables 1–3 using the quantity $\sigma_1 \equiv \sum_{j=1}^{N} |z_j|^2$ as a measure of the solution amplitude. These branches are called *axial*, although the less precise term *maximal* is frequently used. The tables list these (steady) solutions of the equations in the form $(z_1, \ldots, z_N)$, $N = 3$, 4 and 6, respectively, to cubic order. In these tables the variables x and y are taken to be real. Note that Table 3 is constructed for the group $\Gamma \oplus \boldsymbol{Z}_2(-I)$; Table 4 gives the corresponding results when $\boldsymbol{Z}_2(-I)$ is weakly broken (a_{12} small). Tables 1–3 list three, four and 10 primary solution branches; in each case these branch simultaneously from the trivial (spatially uniform) state. Additional primary branches with

Table 2
Maximal isotropy branches for the FCC lattice

Name	Solution	σ_1	Branching equation
Trivial	(0,0,0,0)	0	$\sigma_1 = 0$
Lamellæ	$(x, 0, 0, 0)$	x^2	$\lambda + (h_{1,\sigma_1} + h_3)\sigma_1 = 0$
Rhombic prisms	$(x, x, 0, 0)$	$2x^2$	$\lambda + \frac{1}{2}(2h_{1,\sigma_1} + h_3)\sigma_1 = 0$
FCC	(x, x, x, x)	$4x^2$	$\lambda + \frac{1}{4}(4h_{1,\sigma_1} + h_3 + p_3)\sigma_1 = 0$
Double-diamond	$(-x, x, x, x)$	$4x^2$	$\lambda + \frac{1}{4}(4h_{1,\sigma_1} + h_3 - p_3)\sigma_1 = 0$

Table 3
Maximal isotropy branches for the BCC lattice with the extra $\boldsymbol{Z}_2(-I)$ symmetry

Name	Solution	σ_1	Branching equation
Trivial	(0,0,0,0,0,0)	0	$\sigma_1 = 0$
Lamellæ	$(x, 0, 0, 0, 0, 0)$	x^2	$\lambda + a_1\sigma_1 = 0$
Rhombs	$(x, x, 0, 0, 0, 0)$	$2x^2$	$\lambda + \frac{1}{8}(4a_1 + a_3)\sigma_1 = 0$
Squares	$(x, 0, 0, x, 0, 0)$	$2x^2$	$\lambda + \frac{1}{2}(a_1 + a_8)\sigma_1 = 0$
Hex	$(0, 0, 0, x, x, x)$	$3x^2$	$\lambda + \frac{1}{6}(2a_1 + a_3)\sigma_1 = 0$
Tri	$i(0, 0, 0, x, x, x)$	$3x^2$	$\lambda + \frac{1}{6}(2a_1 + a_3)\sigma_1 = 0$
BCC	(x, x, x, x, x, x)	$6x^2$	$\lambda + \frac{1}{6}(a_1 + a_3 + a_8 + a_{16})\sigma_1 = 0$
BCCI	$i(x, x, x, x, x, x)$	$6x^2$	$\lambda + \frac{1}{6}(a_1 + a_3 + a_8 - a_{16})\sigma_1 = 0$
123	$(x, x, x, 0, 0, 0)$	$3x^2$	$\lambda + \frac{1}{6}(2a_1 + a_3)\sigma_1 = 0$
A	$(0, x, x, 0, -x, x)$	$4x^2$	$\lambda + \frac{1}{8}(2a_1 + a_3 + 2a_8 - a_{16})\sigma_1 = 0$
B	$(0, x, x, 0, x, x)$	$4x^2$	$\lambda + \frac{1}{8}(2a_1 + a_3 + 2a_8 + a_{16})\sigma_1 = 0$

Table 4
The maximal isotropy branches of Table 3 when the reflection symmetry $\boldsymbol{Z}_2(-I)$ is broken. Of the original ten branches six remain as primary branches

Name	Solution	σ_1	Branching equation
Trivial	(0,0,0,0,0,0)	0	$\sigma_1 = 0$
Lamellæ	$(x, 0, 0, 0, 0, 0)$	x^2	$\lambda + a_1x^2 = 0$
Rhombs′	$(x, x, 0, 0, 0, y)$	$2x^2 + y^2$	$\lambda + \frac{1}{4}[(4a_1 + a_3)x^2 + 2a_{12}y + a_3y^2] = 0$, $y = 2a_{12}/(4a_1 - a_3)$
Squares	$(x, 0, 0, x, 0, 0)$	$2x^2$	$\lambda + (a_1 + a_8)x^2 = 0$
Hex	$(0, 0, 0, x, x, x)$	$3x^2$	$\lambda + \frac{1}{2}[a_{12}x + (2a_1 + a_3)x^2] = 0$
Tri′	$(0, 0, 0, z, z, z)$	$3x^2 + 3y^2$	$\lambda + \frac{1}{2}[(2a_1 + a_3)\lvert z\rvert^2 - a_{23}\lvert z\rvert^4 + 2a_{24}x(x^2 - 3y^2)] = 0$,
	$z = x + \mathrm{i}y \in \boldsymbol{C}$		$y^2 = [a_{12} + (a_{13} + a_{15} - a_{24})x^2 + 2a_{23}x^3]/(-a_{13} - a_{15} + a_{24} + 6a_{23}x)$
BCC	(x, x, x, x, x, x)	$6x^2$	$\lambda + a_{12}x + (a_1 + a_3 + a_8 + a_{16})x^2 = 0$
BCCI	$i(x, x, x, x, x, x)$	$6x^2$	$\lambda + (a_1 + a_3 + a_8 - a_{16})x^2 = 0$
123′	(x, x, x, y, y, y)	$3x^2 + 3y^2$	$\lambda + \frac{1}{2}[(2a_1 + a_3)x^2 + 2a_{12}y + (a_3 + 2a_8 + 2a_{16})y^2] = 0$, $y = a_{12}/(2a_1 - 2a_8 - 2a_{16})$
A	$(0, x, x, 0, -x, x)$	$4x^2$	$\lambda + \frac{1}{2}(2a_1 + a_3 + 2a_8 - a_{16})x^2 = 0$
B′	(y, x, x, y, x, x)	$4x^2 + 2y^2$	$\lambda + \frac{1}{2}[(2a_1 + a_3 + 2a_8 + a_{16})x^2 + 2a_{12}y + (a_3 + a_{16})y^2] = 0$, $y = 2a_{12}/(2a_1 - a_3 + 2a_8 - a_{16})$

submaximal isotropy ($\dim \mathrm{Fix}(\Sigma) > 1$) are present on the FCC and BCC lattices [14,19] but these are most likely always unstable and are omitted. A pictorial representation of the most interesting primary solutions can be found in [14]. In the BCC case only six primary branches remain once the $\boldsymbol{Z}_2(-I)$ symmetry is broken, with four branches becoming secondary. In Table 4 these are indicated by a prime. Note that the branch labeled tri′ requires fifth order terms (with coefficients a_{13}, a_{15}, a_{23} and a_{24}, listed in [14]) for its specification. We do not calculate these terms in this paper. Additional branches (called **1** ′–**5** ′ in [14]), arising from submaximal primary branches for the group $\Gamma \oplus \boldsymbol{Z}_2(-I)$, are omitted.

The stability properties of all these solutions for the three lattices have been determined as a function of the coefficients [14]. These calculations summarize stability properties with respect to perturbations on the particular lattice used, i.e., they establish *instability* but because they do not consider all possible perturbations they cannot establish strict *stability*. In the following we compute the necessary coefficients for the two models under consideration.

3. The Brusselator model

We have performed the center manifold reduction for the Brusselator model (1) on the SC, FCC and BCC lattices (see Appendix A). This system has a uniform equilibrium at $(X, Y) = (A, B/A)$. Traditionally, B is chosen as the bifurcation parameter. For $B < B_{\mathrm{H}} \equiv 1 + A^2$ this uniform state is stable with respect to oscillatory perturbations. At $B = B_{\mathrm{H}}$, the system undergoes a Hopf bifurcation to a periodic state with wavenumber $k = 0$ (see Fig. 1). For

$$B < B_{\mathrm{T}} \equiv \left[1 + A\sqrt{\frac{D_x}{D_y}}\right]^2$$

the uniform state is stable with respect to stationary perturbations. At $B = B_{\mathrm{T}}$, the system undergoes a steady-state bifurcation to a Turing pattern with critical wavenumber k_{T} given by

$$k_{\mathrm{T}}^2 = \frac{A}{\sqrt{D_x D_y}}$$

(see Fig. 1). We define the new parameter

$$R \equiv D_x k_{\mathrm{T}}^2 = A\sqrt{\frac{D_x}{D_y}}, \tag{7}$$

so that $B_{\mathrm{T}} = (1 + R)^2$. In order to see the Turing instability we must have $B_{\mathrm{T}} < B_{\mathrm{H}}$; this requires

$$R(R + 2) < A^2.$$

We also need to know the quantity λ which appears in Eqs. (4)–(6). If $\xi(B)$ is the eigenvalue that vanishes at $B = B_{\mathrm{T}}$, then a Taylor expansion gives us

$$\lambda = \left.\frac{\mathrm{d}\xi}{\mathrm{d}B}\right|_{B=B_{\mathrm{T}}} (B - B_{\mathrm{T}}) = \frac{A^2}{(A^2 - R^2)(R + 1)}(B - B_{\mathrm{T}}). \tag{8}$$

3.1. Results

1. For the SC lattice, we obtain

$$h_{1,\sigma_1} = \Delta(16 - 12R - 26R^2 + 16R^3), \qquad h_3 = \tfrac{1}{9}\Delta(-136 + 70R + 229R^2 - 136R^3),$$

where

$$\Delta \equiv \frac{A^4}{R(1 + R)(A^2 - R^2)^2}. \tag{9}$$

We note from Eq. (4), however, that a simple rescaling of the amplitudes ($z_j \to \zeta z_j$) results in a rescaling of Δ ($\Delta \to \Delta/\zeta^2$). Thus the magnitude of Δ is irrelevant; the bifurcation diagrams depend only upon the sign

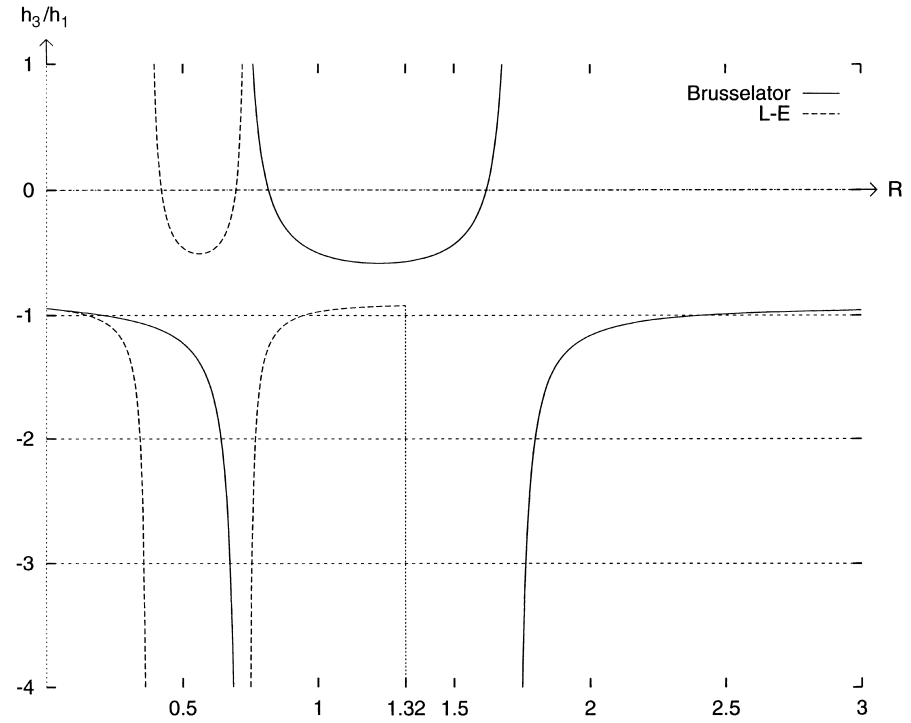

Fig. 2. The ratio of cubic coefficients $h_3/h_{1,\sigma_1}$ as a function of R for the Brusselator (solid) and Lengyel–Epstein (dashed) models. Also shown are the degeneracy conditions $h_3/h_{1,\sigma_1} = 0, -1, -2, -3$.

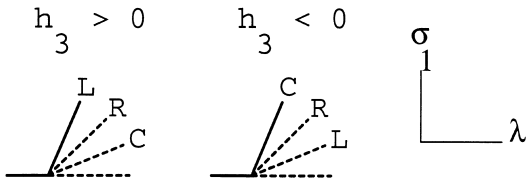

Fig. 3. The bifurcation diagrams σ_1 versus λ containing stable solutions on the simple cubic lattice. Here L, R and C denote the branches of lamellæ, rhombs and simple cubes, respectively. Stable solutions are denoted by a solid line. The first diagram corresponds to $h_{1,\sigma_1} + h_3 < 0, h_3 > 0$, while the second corresponds to $3h_{1,\sigma_1} + h_3 < 0, h_3 < 0$.

of h_3 and the ratio $h_3/h_{1,\sigma_1}$. We plot this ratio (solid curve) as a function of R in Fig. 2, together with the degeneracy conditions $h_3/h_{1,\sigma_1} = 0, -1, -2, -3$. The curve starts with $h_3 < 0$ at $R = 0$. The bifurcation diagrams containing stable solutions are shown in Fig. 3. As a result, both lamellæ and the simple cubic pattern can be stable for appropriate ranges of R: the lamellæ are stable for $0.818 < R < 1.621$ while the cubic pattern is stable for $0.675 < R < 0.818$ and $1.621 < R < 1.763$. We note that the quantity $h_{1,\sigma_1} + h_3$ has been calculated before (see Appendix B of [20]).

2. For the FCC lattice, we obtain

$$h_{1,\sigma_1} = \tfrac{1}{25}\Delta(1296 - 1036R - 1706R^2 + 1296R^3),$$
$$h_3 = \tfrac{1}{225}\Delta(-11464 + 8374R + 15229R^2 - 11464R^3),$$
$$p_3 = \Delta(144 - 108R - 186R^2 + 144R^3).$$

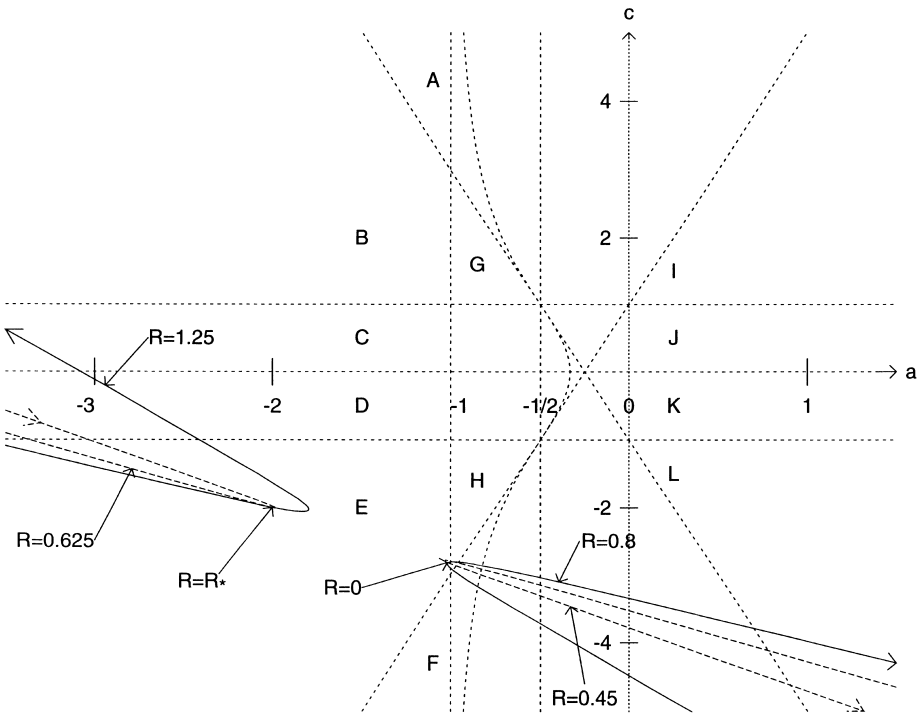

Fig. 4. The (a, c) parameter plane for the FCC lattice showing the regions with different bifurcation diagrams. The solid (dashed) line indicates the location of the Brusselator (Lengyel–Epstein) model as a function of R, with R increasing in the direction of the arrows. For the right branch $h_3 < 0$ for both models, while for the left branch $h_3 > 0$. The points $R = 0, 0.8, 1.25$ for the Brusselator and $R = 0.45, 0.625$ for the Lengyel–Epstein model are indicated, as is $R = R_*$ for both models.

The bifurcation diagrams depend only upon the sign of h_3 and the ratios

$$a \equiv \frac{h_{1,\sigma_1}}{h_3}, \qquad c \equiv \frac{p_3}{h_3}.$$

We show the resulting a-c plane in Fig. 4, together with the curve (solid line) traced out by the coefficients as R increases. The curve starts with $h_3 < 0$ at $R = 0$ at the vertex near $(a, c) = (-1, -3)$ and follows the solid line in the direction indicated by the arrow. After exiting the plot at the right it reenters at the left, and eventually re-enters again from the right, closing up when R reaches ∞. The resulting curve enters a number of regions in the a-c plane containing bifurcation diagrams with stable solution branches. These are shown in Fig. 5. We note that the transformation $c \to -c$ has the sole effect of interchanging the FCC and double-diamond solutions in the bifurcation diagrams. Thus in Fig. 5 we show only the diagrams for $c > 0$; the corresponding diagrams for regions D, E, F, H, K and L are obtained from those for regions C, B, A, G, J and I, respectively, by switching the FCC and double-diamond branch labels. An unstable submaximal primary branch is omitted from these diagrams [19]. From these computations we conclude that lamellæ are stable for $0.894 < R < 1.297$, the FCC state is stable for $0.855 < R < 0.907$ and $1.265 < R < 1.329$, and the double-diamond state is stable for $0.925 < R < 1.228$.

3. Finally, for the BCC lattice, we find that

$$a_{12} = \frac{2A^3(R-1)}{\sqrt{R+1}(A^2 - R^2)^{3/2}}.$$

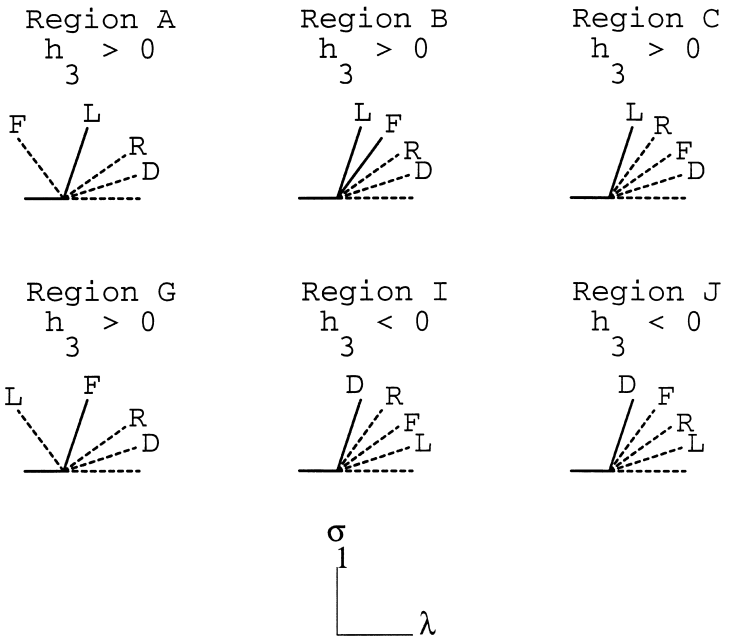

Fig. 5. The six bifurcation diagrams σ_1 versus λ (with $c > 0$) containing stable solutions on the FCC lattice, labeled by region. Here L, R, F and D denote the branches of lamellæ, rhombs, FCC and double-diamond, respectively. The stable branches are denoted by a solid line. In regions B and I of Fig. 4 the relative amplitude of the lamellæ and FCC branches depends upon c. We assume in these cases that $1 < c < 3$. For $c < 0$ the diagrams are the same, but with the labels F and D reversed.

This term too is altered by a rescaling of the amplitudes, but the quantity

$$\nu \equiv \frac{a_{12}^2}{\Delta} = \frac{4A^2R(R-1)^2}{(A^2-R^2)} \tag{10}$$

is not. This scale-invariant quantity is therefore suitable for the construction of the bifurcation diagram. The expansion to third order is only valid when a_{12} is small, i.e., when $R \approx R_* = 1$.

When this is the case, the coefficients of the cubic terms are given by

$$\{a_1, a_3, a_8, a_{16}\} \approx -3\Delta\{1, 8, 2, 4\} = -\frac{3A^4}{2(A^2-1)^2}\{1, 8, 2, 4\}.$$

There is thus only one bifurcation diagram, shown in scale-invariant form in Fig. 6, with solid lines indicating stable branches and broken lines unstable ones. In contrast to Figs. 3 and 5, we do not plot σ_1 versus λ, but instead plot one of the components of each solution versus λ. Specifically, for each primary branch we plot the amplitude x given in Table 4, and for each secondary branch we plot the amplitude y. The figure reveals that when $a_{12} \neq 0$ both BCC and hexagonal prisms bifurcate from the trivial solution in a transcritical bifurcation and are unstable near onset. Both, however, acquire stability at secondary bifurcations, the former at a saddle-node bifurcation and the latter by shedding a branch of unstable states called $123'$. Thus, in contrast to the BCC state the hexagonal prisms do not acquire stability at a secondary saddle-node bifurcation. In fact the BCC state is the only stable state present for $\lambda < 0$. Consequently we might expect to see the BCC state at or just below onset. The BCC state loses stability again at larger amplitude in a transcritical bifurcation involving the $123'$ branch, resulting in a hysteretic transition to the hexagonal prism state. With increasing amplitude this state also loses stability, this time in a transcritical bifurcation involving the state rhomb$'$. This loss of stability results in

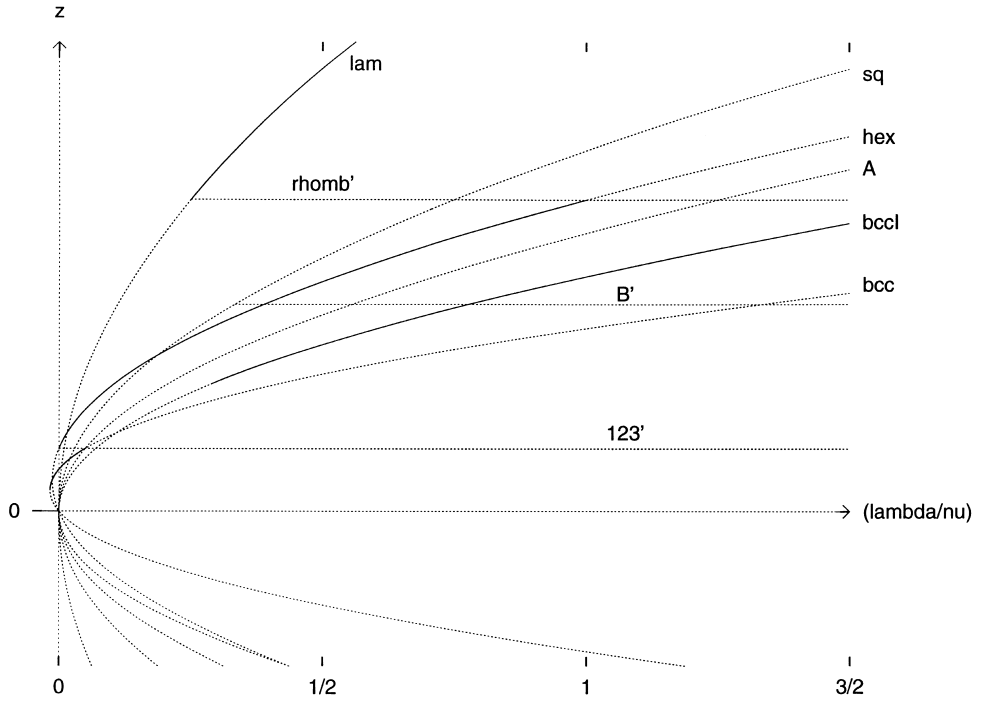

Fig. 6. The bifurcation diagram z versus λ for the BCC lattice near $R = R_*$. For clarity, we plot the amplitude of one of the components of each branch instead of σ_1 (see text). Solid (dashed) lines indicate stable (unstable) solutions. The branch tri′ depends upon fifth order terms and is omitted. The branches shown coexist with the double diamond state (not shown), which is stable on the FCC lattice from onset.

Table 5
Regions of stability for each of the stable solutions. Here 'SC'=simple cubic and 'dd'=double-diamond

Name	Regions of stability		
	Brusselator		Lengyel–Epstein
SC	$0.675 < R < 0.818 \quad 1.621 < R < 1.763$		$0.357 < R < 0.421 \quad 0.697 < R < 0.756$
Lamellæ	$0.894 < R < 1.297$		$0.493 < R < 0.650$
FCC	$0.855 < R < 0.907 \quad 1.265 < R < 1.329$		$0.475 < R < 0.503 \quad 0.642 < R < 0.667$
dd	$0.925 < R < 1.228$		$0.515 < R < 0.632$
Lamellæ	$R \approx 1$	$\nu/4 < \lambda$	$R \approx \sqrt{21} - 4 = 0.583$
Hex	$R \approx 1$	$0 < \lambda < \nu$	$R \approx \sqrt{21} - 4 = 0.583$
BCC	$R \approx 1$	$-\nu/60 < \lambda < \nu/20$	$R \approx \sqrt{21} - 4 = 0.583$
BCCI	$R \approx 1$	$7\nu/24 < \lambda$	$R \approx \sqrt{21} - 4 = 0.583$

a hysteretic transition to either stable lamellæ or stable BCCI which remain stable with increasing λ. Note that at large amplitude two stable branches coexist; which is realized depends on initial conditions. The ranges of λ with stable solutions are summarized in Table 5. As shown below this sequence of transitions is universal for two-species activator-inhibitor systems in the regime where the truncated amplitude equations apply.

Note that when $R \approx 1$ the FCC calculation shows that the double-diamond state bifurcates stably from the trivial state. Unfortunately, the present formulation of the pattern formation problem does not permit us to discuss the relative stability between patterns on different lattices. Empirically, however, solutions found by these techniques are often found to be stable with respect to perturbations on other lattices, although they can be distorted by long-wavelength instabilities. This is so, for example, for the square and hexagonal patterns identified in a two-

dimensional version of this analysis [11]; these patterns have long been observed in a wide variety of experiments. In three dimensions, the BCC structure has been found in the numerical studies of [8], while the double-diamond has been seen in simulations of optical Turing structures in [21], where it is called the tetragonal structure. Experiments on block copolymer melts also show double-diamond-like structures [22].

4. The Lengyel–Epstein model

The center manifold reduction can be applied equally easily to the Lengyel–Epstein model (2). This system has a uniform equilibrium at $(X, Y) = (a/5, 1 + (a/5)^2)$. Traditionally, b is chosen as the bifurcation parameter. For

$$b > b_{\mathrm{H}} \equiv \frac{3a^2 - 125}{5a\delta}$$

this uniform state is stable with respect to oscillatory perturbations. At $b = b_{\mathrm{H}}$, the system undergoes a Hopf bifurcation to a periodic state with wavenumber $k = 0$. For

$$b > b_{\mathrm{T}} \equiv \frac{[125 + 13a^2 - 4a\sqrt{10(25 + a^2)}]c}{5a}$$

the uniform state is stable with respect to stationary perturbations. At $b = b_{\mathrm{T}}$, the system undergoes a steady-state bifurcation to a Turing pattern with critical wavenumber k_{T} given by

$$k_{\mathrm{T}}^2 = -5 + \sqrt{\frac{40a^2}{25 + a^2}}.$$

Because of this relationship, we can choose to treat k_{T}^2 as a parameter instead of a. This simplifies many of our results. In order to emphasize the similarities between the Lengyel–Epstein and Brusselator models, we define

$$R \equiv k_{\mathrm{T}}^2.$$

For the Lengyel–Epstein model, space has already been scaled to make the activator diffusivity equal to one. Thus this definition is completely analogous to Eq. (7) for the Brusselator. We will continue to refer to R as the (square of the) wavenumber.

Since $k_{\mathrm{T}}^2 > 0$ we must have $a > 5\sqrt{5/3} \approx 6.45$. The maximum attainable critical wavenumber is $R = k_{\mathrm{T}}^2 = 2\sqrt{10} - 5 \approx 1.32$. In order to see the Turing instability, we must have $b_{\mathrm{T}} > b_{\mathrm{H}}$, which requires

$$c\delta > \frac{3a^2 - 125}{125 + 13a^2 - 4a\sqrt{10(25 + a^2)}} = 1 + \frac{10}{R}.$$

The coefficient λ is given by

$$\lambda = -\frac{5\delta(R + 5)^2}{8a(c\delta - 1)R}(B - B_{\mathrm{T}}). \tag{11}$$

4.1. Results

1. The results for the SC lattice are

$$h_{1,\sigma_1} = 4\Delta(500 - 1775R + 890R^2 + 711R^3 + 120R^4 + 6R^5),$$
$$h_3 = -\tfrac{2}{9}\Delta(8500 - 28275R + 13970R^2 + 11647R^3 + 1968R^4 + 98R^5),$$

where

$$\Delta \equiv \frac{25c\delta(R+5)}{32a(c\delta-1)^2R^2}$$

is again irrelevant, except for the sign. We plot the ratio $h_3/h_{1,\sigma_1}$ as a function of R in Fig. 2 in the form of a dashed line. The curve starts with $h_3 < 0$ at $R = 0$. The lamellæ are stable for $0.421 < R < 0.697$ and the cubic pattern is stable for $0.357 < R < 0.421$ and $0.697 < R < 0.756$.

2. For the FCC lattice,

$$\begin{aligned} h_{1,\sigma_1} &= \tfrac{4}{25}\Delta(40500 - 128875R + 64610R^2 + 49391R^3 + 8064R^4 + 394R^5), \\ h_3 &= -\tfrac{2}{225}\Delta(716500 - 2227875R + 1111730R^2 + 860263R^3 + 140352R^4 + 6842R^5), \\ p_3 &= 12\Delta(1500 - 4625R + 2310R^2 + 1773R^3 + 288R^4 + 14R^5). \end{aligned}$$

We show the curve traced out in a-c parameter space in Fig. 4, again as a dashed line. Broadly speaking, the curve looks like the corresponding curve for the Brusselator (solid line). The curve starts with $h_3 < 0$ just to the left of $a = -1$ where $R = 0$; however, with increasing R the system describes the dashed curve in a direction opposite to that for the Brusselator with increasing R. Moreover, the curve does not close up: a small gap is present near the vertex $(a, c) = (-1, -3)$. The lamellæ are stable for $0.493 < R < 0.650$, the FCC state is stable for $0.475 < R < 0.503$ and $0.642 < R < 0.667$, and the double-diamond state is stable for $0.515 < R < 0.632$.

3. For the BCC lattice, we have

$$a_{12}^2 = \frac{125c^2\delta^2(R+5)(-5+8R+R^2)^2}{8a(c\delta-1)^3R}.$$

The ratio

$$\nu \equiv \frac{a_{12}^2}{\Delta} = \frac{20c\delta R(-5+8R+R^2)^2}{c\delta-1} \tag{12}$$

is again invariant under rescaling of the amplitudes. Again, we seek a_{12} very small, so our analysis is only valid for $R \approx R_* = \sqrt{21} - 4$. In this case we have

$$\{a_1, a_3, a_8, a_{16}\} \approx -60\Delta(13\sqrt{21} - 57)\{1, 8, 2, 4\} = -\frac{75\sqrt{18 - 2\sqrt{21}}(3 + \sqrt{21})c\delta}{8(c\delta-1)^2}\{1, 8, 2, 4\}$$

and the cubic coefficients are again in the special ratio 1:8:2:4 found for the Brusselator model. This is not an accident. It is possible to show that this is a generic property of two-species systems of reaction–diffusion equations with identical nonlinearities (see Appendix A). Thus such systems are generically described by the bifurcation diagram in Fig. 6 in the limit of small a_{12}. We remark that the special wavenumber k_* appears on the FCC lattice as well where it defines the intersection of the dashed (Lengyel–Epstein) and solid (Brusselator) curves at $(a, c) = (-2, -2)$.

5. Discussion

In this paper we have analyzed the types of patterns that may arise near onset of a steady-state Turing instability in an isotropic homogeneous system of reaction–diffusion equations in three dimensions. Explicit predictions were made for two models of interest, the Brusselator and the Lengyel–Epstein model. These predictions involve

not only the spatially periodic patterns that are possible on the three lattices considered but also their stability properties with respect to perturbations on these lattices. There are several points of similarity between the Brusselator and Lengyel–Epstein models, some expected and some not. These are easier to see if we note first that in the Lengyel–Epstein model space has already been scaled so that the activator has diffusivity equal to one. If we do the same for the Brusselator, i.e., set $D_x = 1$, then both models have only three independent parameters (the Lengyel–Epstein model is described by the three parameters a, δb and δc). One of these is determined by the requirement that we have a bifurcation, and another can be eliminated by rescaling the (perturbation) amplitudes. Thus it comes as no surprise that the types of possible bifurcations for each model are characterized by a single parameter, which we have denoted by R.

What is perhaps more unexpected is that the two models trace out very similar curves in parameter space (see Figs. 2 and 4). In fact, the two curves of Fig. 4 both pass through the point $(a, c) = (-2, -2)$. This is a result of the surprising fact that for each model there is a special wavenumber

$$k_*^2 = \begin{cases} 1/D_x, & \text{Brusselator} \\ \sqrt{21} - 4, & \text{Lengyel–Epstein} \end{cases}$$

for which the quadratic term on the BCC lattice vanishes. At this wavenumber, the cubic coefficients for each lattice take on fixed ratios, *independent of the model*. This is a generic feature of two-species chemical reaction–diffusion models with identical nonlinearities, as shown in Appendix A. The Schnakenberg model [23], not discussed here, provides another frequently studied system of this type. Such systems are a natural consequence of the law of mass action in systems involving a single activator and a single inhibitor. Consequently this universality is a property of a large class of useful models. However, there are two-species models, such as that put forward in [24], for which k_* does *not* exist.

We summarize in Table 5 the stable solutions on the three lattices and their stability ranges for each model. In the first half we list solutions defined on the SC and FCC lattices, and give the ranges in R for which they are stable. Note that for, e.g., the simple cubic solution, we can only determine its stability with respect to perturbations defined on the SC lattice. Thus, strictly speaking, we have proved that this solution is *unstable* for R *outside* the given intervals. The same, of course, goes for the FCC and double-diamond solutions. As the lamellæ are defined on both the SC and FCC lattices, the range of R-values given is for stability with respect to perturbations defined on either lattice. For each of these solutions, the given branch is stable wherever it exists, i.e., for all $\lambda > 0$.

In the second half of the table we list stable solutions on the BCC lattice. For this lattice, all solutions are unstable for R sufficiently far from the special values specified. For $R \approx R_*$, we show the range in λ for which each solution is stable. These ranges depend upon the model only through the definitions of ν, given by Eq. (10) for the Brusselator and Eq. (12) for the Lengyel–Epstein model. Note that in the interval $7\nu/24 < \lambda < \nu$ there are four (including the double diamond on the FCC lattice) solutions which are stable simultaneously.

There are few numerical simulations of activator-inhibitor systems in three dimensions, and no detailed experiments. We are aware only of two sets of numerical results, both for the Brusselator model [8,9]. Other simulations emphasize effects of gradients in the input concentration over the three-dimensional structures that form; such inhomogeneities or pinning at boundaries can stabilize additional structures not described by the present theory, such as the Scherck state discussed in [9]. The existing Brusselator simulations both use $R = 1.59$ but involve different Turing wavenumbers because of the different diffusion coefficients used: $k_T = 1.261$ in [8] and $k_T = 0.892$ in [9]. Our theory does not find any stable states near onset for this value of R (cf. Table 5), a result that is consistent with the simulations. Instead, De Wit et al. [8] found a sequence of transitions from a finite amplitude BCC state to hexagonal prisms and then to lamellæ, as B is increased beyond B_T. To explain the observed transitions they appeal to a theory of the type described here but their bifurcation diagrams omit a number of primary and secondary branches and with them several important stability changes that take place at finite amplitude. Moreover, as we have

seen in the present paper, such a theory only applies when $R \approx 1$, and even then some fifth order terms may have to be retained. For the value of R used in the simulations ($R = 1.59$) the truncation of the amplitude equations at third order cannot be justified, and the resulting predictions (such as the prediction that the hexagonal prisms acquire stability at the saddle-node bifurcation) must be considered unreliable. Indeed, as shown in Fig. 6, in the regime of validity of the truncated equations the hexagonal prisms acquire stability via a different secondary bifurcation. The explicit reduction performed here suggests new parameter ranges that could prove rewarding for future simulations of activator-inhibitor systems, and in which quantitative comparisons between amplitude equations and simulations could be performed.

Acknowledgements

This work was supported by the National Science Foundation under grant DMS-9703684.

Appendix A. The center manifold reduction

In this Appendix we describe the procedure by which we reduce a system of partial differential equations to a finite-dimensional system of ordinary differential equations we call amplitude equations. We start with a general Turing system for M chemical species for which $X^h = 0$ is an equilibrium:

$$\dot{X}^h(\boldsymbol{x}, t) = D^h \nabla^2 X^h + A^{h,i} X^i + A^{h,ij} X^i X^j + A^{h,ijk} X^i X^j X^k + \cdots,$$

where the indices h, i, j and k run through the M species, and we have employed the Einstein summation convention, except in the diffusion term, paying no regard to co-or contravariance. Also, we define the $A^{h,ij}$, etc. so that they are fully symmetric under permutations of all their indices after the comma.

We impose periodic boundary conditions in all three directions, and then write

$$X^h(\boldsymbol{x}, t) = \sum_{l \in L} \tilde{X}^h_l(t)\, \mathrm{e}^{\mathrm{i}\boldsymbol{k}_l \cdot \boldsymbol{x}},$$

where L is the set of lattice points, indexed by l. We can scale space so that the coordinates of points in L are all integers. We will use indices l and beyond in the alphabet to denote points in the lattice L. In addition, to avoid confusion, we write all species indices as superscripts and all lattice point indices as subscripts.

Substituting this into the previous equation, using the discrete convolution theorem and dropping the tildes, we get

$$\dot{X}^h_l = -D^h |\boldsymbol{k}_l|^2 X^h_l + A^{h,i} X^i_l + A^{h,ij} \sum_{l_1+l_2=l} X^i_{l_1} X^j_{l_2} + A^{h,ijk} \sum_{l_1+l_2+l_3=l} X^i_{l_1} X^j_{l_2} X^k_{l_3} + \mathcal{O}(X^4).$$

To find the normal modes we first diagonalize the linear matrix

$$J^{h,i}_l = -D^h k_l^2 \delta^{h,i} + A^{h,i}.$$

For each l we choose a matrix

$$S_l = \begin{pmatrix} \alpha^{11}_l & \cdots & \alpha^{1M}_l \\ \vdots & \ddots & \vdots \\ \alpha^{M1}_l & \cdots & \alpha^{MM}_l, \end{pmatrix}$$

with inverse

$$S_l^{-1} = \{\beta_l^{ij}\},$$

such that $\det(S_l) = 1$ and S_l diagonalizes J_l, so

$$S_l^{-1} J_l S_l = \Lambda_l \equiv \begin{pmatrix} \lambda_l^1 & & \\ & \ddots & \\ & & \lambda_l^M \end{pmatrix}. \tag{A.1}$$

We can do this provided that the eigenvalues λ_l^i are distinct. Generically, this is true for all $l \in L$. For each l we order the eigenvalues so that

$$\operatorname{Re}\lambda_l^1 > \cdots > \operatorname{Re}\lambda_l^M.$$

If two eigenvalues λ_l^i and λ_l^{i+1} have equal real part we order them so that $\operatorname{Im}\lambda_l^i > \operatorname{Im}\lambda_l^{i+1}$. Each S_l depends upon l only through the length $|\boldsymbol{k}_l|$.

We now work in a new basis, defined by

$$\begin{pmatrix} X_l^1 \\ \vdots \\ X_l^M \end{pmatrix} = S_l \begin{pmatrix} W_l^1 \\ \vdots \\ W_l^M \end{pmatrix}.$$

In this new basis we have

$$\dot{W}_l^g = \lambda_l^g W_l^g + \beta_l^{gh} A^{h,ij} \sum_{l_1+l_2=l} \alpha_{l_1}^{ii'} W_{l_1}^{i'} \alpha_{l_2}^{jj'} W_{l_2}^{j'} + \beta_l^{gh} A^{h,ijk} \sum_{l_1+l_2+l_3=l} \alpha_{l_1}^{ii'} W_{l_1}^{i'} \alpha_{l_2}^{jj'} W_{l_2}^{j'} \alpha_{l_3}^{kk'} W_{l_3}^{k'}. \tag{A.2}$$

Let L_0 be the set of those wavevectors which go critical at $B = B_{\mathrm{T}}$. Since we are not considering a Hopf bifurcation, $\lambda_l^1(B = B_{\mathrm{T}}) = 0$ for these lattice points and $\operatorname{Re}\lambda_l^1 < 0$ for every other lattice point. We will use the convention $l \in L$, $m \in L_0$ and $n \in L - L_0$.

The coefficient λ in the amplitude equations (4)–(6) is given by

$$\lambda = (\lambda_m^1)'\Big|_{B=B_{\mathrm{T}}} (B - B_{\mathrm{T}}),$$

where $(\cdot)' = \mathrm{d}(\cdot)/\mathrm{d}B$. A simple calculation, for a two species system, now gives

$$(\lambda_m^1)'\Big|_{B=B_{\mathrm{T}}} = \frac{[\det(J_m)]'}{\operatorname{Tr}(J_m)}\Big|_{B=B_{\mathrm{T}}},$$

yielding the expressions (8) and (11). The coefficients of the nonlinear terms can all be calculated at threshold, and consequently we now set $B = B_{\mathrm{T}}$.

To determine the center manifold, we express each stable amplitude W_l^i (for $i \neq 1$ or $l \notin L_0$) in terms of the critical amplitudes W_m^1. The center manifold is tangent to the subspace of critical amplitudes, so up to quadratic terms we can write, for $i \neq 1$ or $l \notin L_0$,

$$W_l^i = \sum_{m_1,m_2 \in L_0} g_{l,m_1m_2}^i W_{m_1}^1 W_{m_2}^1. \tag{A.3}$$

It follows that

$$\dot{W}_l^i = \sum_{m_1,m_2 \in L_0} g_{l,m_1m_2}^i (W_{m_1}^1 \dot{W}_{m_2}^1 + \dot{W}_{m_1}^1 W_{m_2}^1). \tag{A.4}$$

By Eq. (A.2) we know that $\dot{W}^1_{m_1}$ contains no terms linear in the W^1_m's, so Eq. (A.4) must vanish to $\mathcal{O}((W^1_m)^2)$. Thus Eq. (A.2) for the stable modes gives us

$$\mathcal{O}((W^1_m)^2):\ 0=\lambda^g_l\sum_{m_1,m_2\in L_0} g^g_{l,m_1m_2}W^1_{m_1}W^1_{m_2}+\beta^{gh}_l A^{h,ij}\sum_{m_1+m_2=l}\alpha^{i1}_{m_1}W^1_{m_1}\alpha^{j1}_{m_2}W^1_{m_2}.$$

To simplify notation we set $\alpha\equiv\alpha_{m_1}=\alpha_{m_2}$ and $\beta\equiv\beta_{m_1}=\beta_{m_2}$. Thus we can take

$$g^g_{l,m_1m_2}=-\frac{\beta^{gh}_l}{\lambda^g_l}A^{h,ij}\alpha^{i1}\alpha^{j1}\delta_{l,m_1+m_2}. \tag{A.5}$$

Because of the way the elements λ^g_l are defined in Eq. (A.1), this formula is *not* to be summed over g and l. The final δ is the Kronecker δ. In order to simplify our notation below, we set $g^1_{m,m_1m_2}\equiv 0$. We can still use Eq. (A.5) if we set $\lambda^1_m\equiv\infty$ instead of 0.

At this point we substitute the expressions (A.3) for the stable W^i_l back into Eq. (A.4) for $\dot{W}^1_m$. To third order in the W^1_m's we have

$$\begin{aligned}\dot{W}^1_m=\beta^{1h}\Bigg\{&A^{h,ij}\sum_{m_1+m_2=m}\alpha^{i1}\alpha^{j1}W^1_{m_1}W^1_{m_2}\\&+A^{h,ij}\sum_{m_1+l_2=m}\alpha^{i1}\alpha^{jj'}_{l_2}W^1_{m_1}\sum_{m_2,m_3\in L_0}g^{j'}_{l_2,m_2m_3}W^1_{m_2}W^1_{m_3}\\&+A^{h,ij}\sum_{l_1+m_2=m}\alpha^{ii'}_{l_1}\alpha^{j1}W^1_{m_2}\sum_{m_1,m_3\in L_0}g^{i'}_{l_1,m_1m_3}W^1_{m_1}W^1_{m_3}\\&+A^{h,ijk}\sum_{m_1+m_2+m_3=m}\alpha^{i1}\alpha^{j1}\alpha^{k1}W^1_{m_1}W^1_{m_2}W^1_{m_3}\Bigg\}.\end{aligned}$$

Now we shuffle dummy indices and use Eq. (A.5) and the symmetry of A to get

$$\begin{aligned}\dot{W}^1_m=\beta^{1h}\Bigg\{&A^{h,ij}\sum_{m_1+m_2=m}\alpha^{i1}\alpha^{j1}W^1_{m_1}W^1_{m_2}\\&-2A^{h,ij}\sum_{m_1+m_2+m_3=m}\alpha^{i1}\alpha^{jj'}_l\frac{\beta^{j'a}_l}{\lambda^{j'}_l}A^{a,bc}\alpha^{b1}\alpha^{c1}W^1_{m_1}W^1_{m_2}W^1_{m_3}\\&+A^{h,ijk}\sum_{m_1+m_2+m_3=m}\alpha^{i1}\alpha^{j1}\alpha^{k1}W^1_{m_1}W^1_{m_2}W^1_{m_3}\Bigg\},\end{aligned} \tag{A.6}$$

where $l\equiv m_2+m_3$. The sum looks a little unusual in that l and j' appear three times, but this is again due to the way Λ_l is represented in Eq. (A.1).

We have two very different cases: either it is possible (BCC) for two critical wavevectors to add up to a third (so $\sum_{m_1+m_2=m}$ is not trivially 0) or it is not (SC and FCC). In the latter case the first line on the right hand side of Eq. (A.6) vanishes. In the former case we generically have a quadratic term in the final amplitude equations. Cubic terms in the amplitude equations are only relevant when the coefficient of the quadratic term is small. As we will see later, this typically happens for a particular wavenumber $k_{\mathrm{T}}=k_*$ that gives us

$$A^{h,ij}\alpha^{i1}\alpha^{j1}=\{0,0\}. \tag{A.7}$$

In this instance, we see that the middle line of Eq. (A.6) also vanishes. Thus if two critical wavevectors can add up to a third, then we do not need to evaluate the middle line. This is the case for the BCC lattice.

For the SC and FCC lattices, no two critical wavevectors can add up to a third, but we can simplify the l-dependent expressions on this middle line. We know that $l = m_2 + m_3 = n \notin L_0$. Note first that

$$\sum_{j'} \frac{\alpha_n^{jj'} \beta_n^{j'a}}{\lambda_n^{j'}} = (S_n \Lambda_n^{-1} S_n^{-1})^{ja}.$$

Using Eq. (A.1), we get

$$\sum_{j'} \frac{\alpha_n^{jj'} \beta_n^{j'a}}{\lambda_n^{j'}} = (J_n^{-1})^{ja}.$$

Putting everything back together into Eq. (A.6), we obtain

$$\dot{W}_m^1 = \beta^{1h} A^{h,ij} \alpha^{i1} \alpha^{j1} \sum_{m_1+m_2=m} W_{m_1}^1 W_{m_2}^1 + \sum_{m_1+m_2+m_3=m} F(m_2+m_3) W_{m_1}^1 W_{m_2}^1 W_{m_3}^1, \tag{A.8}$$

where

$$F(l) \equiv [-2\beta^{1h} A^{h,ij} \alpha^{i1} (J_l^{-1})^{ja} A^{a,bc} \alpha^{b1} \alpha^{c1} + \beta^{1h} A^{h,ijk} \alpha^{i1} \alpha^{j1} \alpha^{k1}]$$

depends upon l only through the square of the length of l.

A.1. Application to the Brusselator

We can use Mathematica™ to simplify the process of applying this formula to individual models. We start by defining the Brusselator without diffusion:

```
system = {-(B + 1)x + x^2y + A, Bx - x^2y}.
```

The equilibrium solutions are $x = A$ and $y = B/A$. When we redefine x and y to be the deviations from equilibrium, we get

$$\texttt{system} = \begin{pmatrix} (B-1)x + (B/A)x^2 + A^2 y + 2Axy + x^2 y \\ -Bx - (B/A)x^2 - A^2 y - 2Axy - x^2 y \end{pmatrix}$$

We define `z = {x, y}`, and then

```
J=Table[D[system[[h]], z[[i]]], {h, 2}, {i, 2}]
    -k DiagonalMatrix[{Dx, Dy}]/.{x→0, y→0}
Quad = 1/2!Table[D[system[[h]], z[[i]], z[[j]]],
{h, 2}, {i, 2}, {j, 2}]/.{x→0, y → 0}
Cub = 1/3! Table[D[system[[h]], z[[i]], z[[j]], z[[k]]],
    {h, 2}, {i, 2}, {j, 2}, {k, 2}]/.{x → 0, y → 0}
```

For the diffusion terms in `J` we have used `k` instead of `k^2`. We would like to be able to differentiate with respect to k^2, so we have `k` $= k^2$. Our results so far are

$$\texttt{J} = \begin{pmatrix} -1 + B - D_x k^2 & A^2 \\ -B & -A^2 - D_y k^2 \end{pmatrix}$$

$$\texttt{Quad} = \left\{ \begin{pmatrix} B/A & A \\ A & 0 \end{pmatrix}, \begin{pmatrix} -B/A & -A \\ -A & 0 \end{pmatrix} \right\}$$

$$\texttt{Cub} = \frac{1}{3} \begin{matrix} h \downarrow \end{matrix} \begin{pmatrix} \overset{i \rightarrow}{\begin{pmatrix} 0 & 1 \\ 1 & 0 \end{pmatrix}} & \begin{pmatrix} 1 & 0 \\ 0 & 0 \end{pmatrix} \\ \begin{pmatrix} 0 & -1 \\ -1 & 0 \end{pmatrix} & \begin{pmatrix} -1 & 0 \\ 0 & 0 \end{pmatrix} \end{pmatrix}.$$

We remove the distance scale by substituting

```
J = J/.{Dx → R/kT, Dy → T/kT, k → r kT}
```

(kT is k_{T}^2) so that

$$J = \begin{pmatrix} -1 + B - rR & A^2 \\ -B & -A^2 - rT \end{pmatrix}.$$

Because $r = k^2/k_{\mathrm{T}}^2$, r is proportional to the square of the length of the lattice point l corresponding to $\boldsymbol{k}$. The critical wavevectors are those with $k = k_{\mathrm{T}}$, i.e., $r = 1$; k_{T} is the critical wavenumber in the absence of boundaries or that at which $B(k)$ reaches a minimum. We assume that, if there are boundaries, they are such as to allow k_{T} into the discrete spectrum.

We choose B to be the distinguished bifurcation parameter. We find its critical value $B(k)$ for each wavevector by taking

```
subb = Solve[Det[J] == 0, B][[1]]
```

and getting

$$\{\texttt{B} \rightarrow \frac{\texttt{A\^{}2} + \texttt{A\^{}2r R} + \texttt{r T} + \texttt{r\^{}2R T}}{\texttt{r T}}\};$$

$B(k)$ reaches a minimum at $k = k_{\mathrm{T}}$ (or $B(r)$ reaches a minimum at $r = 1$), so we differentiate the result with respect to r, set $r = 1$, and set the result to 0 to get

$$A^2 = RT.$$

We therefore substitute

```
T → A^2/R
```

and let B be the minimum critical value $B_{\mathrm{T}} = B(k_{\mathrm{T}})$ by setting

```
subb = subb/.r → 1
```

so that

```
subb = {B → (R + 1)^2}
```

i.e., $B_{\mathrm{T}} = (R+1)^2$. Altogether we obtain

$$\texttt{J} = \begin{pmatrix} R(2 + R - r) & A^2 \\ -(1+R)^2 & -A^2(R+r)/R \end{pmatrix}, \qquad \texttt{Quad} = \left\{ \begin{pmatrix} (1+R)^2/A & A \\ A & 0 \end{pmatrix}, \begin{pmatrix} -(1+R)^2/A & -A \\ -A & 0 \end{pmatrix} \right\}.$$

We can now find the transformation matrix S and the vectors α^{a1} and β^{1h} for the critical wavevectors by taking

```
eig = Eigensystem[J/. r → 1]
```

```
S = Transpose[eig[[2]]]/Sqrt[Det[eig[[2]]]
Si = Inverse[S]
a1 = Transpose[S][[1]]; b1 = Si[[1]]
```

We may need to provide Mathematica™ with some guidance throughout this step, as `eig[[2]]` may have a negative determinant, or the square root may not appear as we wish, or its null eigenvector may not appear as the first row. In this case we may use the fact that

$$T > R > 0 \qquad \Rightarrow \qquad 0 < R < A.$$

Mathematica™ always reads consecutive dot products from left to right, and always sums over the last index of the left operand and the first index of the right operand. Using the symmetry of the A tensors, all we need to do now is set

```
quadratic = b1.Quad.a1.a1
```
(A.9)

```
F[r_] := Evaluate[Simplify[-2b1.Quad.a1.Inverse[J].Quad.a1.a1 + b1.Cub.a1.a1.a1]]
```
(A.10)

The answers for the Brusselator are

$$\texttt{quadratic} = \frac{A^3(R-1)}{(A^2-R^2)^{3/2}\sqrt{1+R}}, \quad F(r) = \left[\frac{A^4}{R(1+R)(A^2-R^2)^2}\right]\frac{2rR^3+(1-2r-r^2)R^2-2R+2r}{(r-1)^2}.$$

Note that the term in square brackets is just Δ in Eq. (9). This concludes the general discussion.

A.2. The cubic lattices

At this point we start looking at specific lattices, starting with the simple cubic. Here

$$L_0 = \{(\pm 1, 0, 0), (0, \pm 1, 0), (0, 0, \pm 1)\},$$

and

$$r = |n|^2.$$

No two critical wavevectors add up to a third so there are no quadratic terms. The general equivariant system for the SC lattice is

$$\dot{z}_1 = \lambda z_1 + h_{1,\sigma_1}(|z_1|^2 + |z_2|^2 + |z_3|^2)z_1 + h_3|z_1|^2 z_1 + \mathcal{O}(\boldsymbol{z}^5).$$

We consider first the coefficient of $|z_2|^2 z_1$, namely h_{1,σ_1}. The terms in Eq. (A.8) which contribute to this are $m_1 = (1, 0, 0), m_2 = (0, 1, 0), m_3 = (0, -1, 0)$ and permutations. Of these six possibilities, two have $|m_2 + m_3|^2 = 0$ and four have $|m_2 + m_3|^2 = 2$. Thus

$$h_{1,\sigma_1} = 2F(0) + 4F(2).$$

Similarly, the coefficient of $|z_1|^2 z_1$ is $h_{1,\sigma_1} + h_3$. This case includes $m_1 = m_2 = (1, 0, 0), m_3 = (-1, 0, 0)$ and permutations. Of these three possibilities, two have $|m_2 + m_3|^2 = 0$ and one has $|m_2 + m_3|^2 = 4$. Thus

$$h_{1,\sigma_1} + h_3 = 2F(0) + F(4) \qquad \Rightarrow \qquad h_3 = 2F(0) + F(4) - h_{1,\sigma_1} = F(4) - 4F(2).$$

For the FCC lattice we have

$$L_0 = \{(\pm 1, \pm 1, \pm 1)\},$$

and

$$r = \frac{|n|^2}{3}.$$

Again, no two critical wavevectors add up to a third, so we have no quadratic terms. Our equivariant system is

$$\dot{z}_1 = \lambda z_1 + h_{1,\sigma_1}(|z_1|^2 + |z_2|^2 + |z_3|^2 + |z_4|^2)z_1 + h_3|z_1|^2 z_1 + p_3 \bar{z}_2 \bar{z}_3 \bar{z}_4 + \mathcal{O}(\boldsymbol{z}^5).$$

Using the same reasoning as before, we get

$$h_{1,\sigma_1} = 2F(0) + 2F(\tfrac{4}{3}) + 2F(\tfrac{8}{3}), \qquad h_3 = F(4) - 2F(\tfrac{4}{3}) - 2F(\tfrac{8}{3}), \qquad p_3 = 6F(\tfrac{4}{3}).$$

For the BCC lattice we have

$$L_0 = \{(\pm 1, \pm 1, 0), (\pm 1, 0, \pm 1), (0, \pm 1, \pm 1)\},$$

for which

$$r = \frac{|n|^2}{2}.$$

Now we can have two critical lattice vectors add up to a third, so $\dot{W}_{m_1}$ does contain terms quadratic in the W_m's. The new system is

$$\begin{aligned}\dot{z}_1 = {} & \lambda z_1 + \tfrac{1}{2}a_{12}(z_2\bar{z}_6 + z_3 z_5) + a_1|z_1|^2 z_1 + \tfrac{1}{4}a_3(|z_2|^2 + |z_3|^2 + |z_5|^2 + |z_6|^2)z_1 \\ & + a_8|z_4|^2 z_1 + \tfrac{1}{2}a_{16}(z_2 z_4 z_5 + z_3 \bar{z}_4 z_6) + \mathcal{O}(\boldsymbol{z}^4).\end{aligned}$$

Comparing with Eq. (A.8), we see at a glance that

$$a_{12} = 2\texttt{quadratic}.$$

For the cubic coefficients, the same reasoning as earlier gives

$$a_1 = 2F(0) + F(4), \quad a_3 = 8F(0) + 8F(1) + 8F(3), \quad a_8 = 2F(0) + 4F(2), \quad a_{16} = 4F(2) + 8F(1).$$

We have only defined $F(r)$ for $r \neq 1$, but we know that our expansion is only useful for $a_{12} \approx 0$. As mentioned after Eq. (A.6), this makes the middle line of Eq. (A.6) vanish, and we have

$$F(r) \approx \beta^{1h} A^{h,ijk} \alpha^{i1} \alpha^{j1} \alpha^{k1}$$

for all r, including $r = 1$. Thus we have

$$a_1 \approx 3F(0), \qquad a_3 \approx 24F(0), \qquad a_8 \approx 6F(0), \qquad a_{16} \approx 12F(0),$$

and hence $a_1{:}a_3{:}a_8{:}a_{16} \approx 1{:}8{:}2{:}4$.

A.3. Universal behavior of two species models on the BCC lattice

We still need to explain the existence of the special wavenumber k_*. Note first from Eq. (1) that the nonlinear (in X and Y) terms in the evolution equations for X and Y are proportional. That is, the term X^2Y appears in both the

$\dot{X}$ and $\dot{Y}$ equations, with a fixed ratio of -1 between them. The Lengyel–Epstein model (2) has the same feature, with a ratio of $\delta b/4$. Thus when we take

$$\texttt{Quad} = 1/2!\,\texttt{Table[D[system[[h]], z[[i]], z[[j]]], \{h, 2\}, \{i, 2\}, \{j, 2\}]/.\{x} \to 0, \texttt{y} \to 0\}$$

we find that the first and second components are proportional. That is,

$$A^{1,ij} \propto A^{2,ij}$$

as matrices. Thus if the first component of the vector `Quad.a1.a1` vanishes, the second must also. Now the matrix $A^{1,ij}$ is symmetric, so its eigenvalues are real. Suppose it has negative determinant. Then it has one positive and one negative eigenvalue, and hence two flat directions, i.e., two linearly independent vectors u^i and v^i such that

$$A^{1,ij}u^i u^j = 0 = A^{1,ij}v^i v^j,$$

so that

$$\texttt{Quad.u.u} = \texttt{Quad.v.v} = \{0, 0\}.$$

These vectors depend upon the model parameters through the matrix $A^{1,ij}$, and hence rotate in the plane as these parameters are changed.

The vector $\alpha^{i1} = \texttt{a1}$ is the right null eigenvector of `J`, and also rotates in the plane as the parameters are varied. It is therefore not surprising that varying k_T can easily cause `a1` to coincide with `u` or `v`. When this happens, we see from Eq. (A.9) that `quadratic` vanishes. More surprisingly, we see from Eq. (A.10) that the parts involving `J` disappear. As `J` is the only place where r appears, the function $F(r)$ becomes independent of r, and the coefficients take on the fixed ratios given.

References

[1] A.M. Turing, The chemical basis of morphogenesis, Phil. Trans. R. Soc. B 237 (1952) 37–72.
[2] J.D. Murray, Mathematical Biology, Springer, Berlin, 1989.
[3] I. Prigogine, R. Lefever, Symmetry breaking instabilities in dissipative systems II, J. Chem. Phys. 48 (1968) 1695–1700.
[4] L.E. Stephenson, D.J. Wollkind, Weakly nonlinear stability analyses of one-dimensional Turing pattern formation in activator–inhibitor/immobilizer model systems, J. Math. Biol. 33 (1995) 771–815.
[5] R. Dillon, P.K. Maini, H.G. Othmer, Pattern formation in generalized Turing systems I, J. Math. Biol. 32 (1994) 345–393.
[6] P. Borckmans, G. Dewel, A. De Wit, D. Walgraef, Turing bifurcations and pattern selection, in: R. Kapral, K. Showalter (Eds.), Chemical Waves and Patterns, Kluwer Academic Publishers, Dordrecht, 1995, pp. 323–363.
[7] D. Walgraef, G. Dewel, P. Borckmans, Nonequilibrium phase transitions and chemical instabilities, Adv. Chem. Phys. 49 (1982) 311–355.
[8] A. De Wit, G. Dewel, P. Borckmans, D. Walgraef, Three-dimensional dissipative structures, Physica D 61 (1992) 289–296.
[9] A. De Wit, P. Borckmans, G. Dewel, Twist grain boundaries in three-dimensional lamellar Turing structures, Proc. Natl. Acad. Sci. USA 94 (1997) 12765–12768.
[10] M. Golubitsky, I. Stewart, D.G. Schaeffer, Singularities and Groups in Bifurcation Theory, vol. II, Springer, Berlin, 1988.
[11] M. Golubitsky, J.W. Swift, E. Knobloch, Symmetries and pattern selection in Rayleigh–Bénard convection, Physica D 10 (1984) 249–276.
[12] C. Hou, M. Golubitsky, An example of symmetry breaking to heteroclinic cycles, J. Diff. Eqs. 133 (1997) 30–48.
[13] B. Dionne, M. Silber, A.C. Skeldon, Stability results for steady, spatially-periodic planforms, Nonlinearity 10 (1997) 321–353.
[14] T.K. Callahan, E. Knobloch, Symmetry-breaking bifurcations on cubic lattices, Nonlinearity 10 (1997) 1179–1216.
[15] I. Lengyel, I.R. Epstein, Modeling of Turing structures in the chlorite–iodide–malonic acid–starch reaction system, Science 251 (1991) 650–652.
[16] V. Castets, E. Dulos, J. Boissonade, P. De Kepper, Experimental evidence of a sustained standing Turing-type nonequilibrium chemical pattern, Phys. Rev. Lett. 64 (1990) 2953–2956.
[17] I. Lengyel, I.R. Epstein, The chemistry behind the first experimental chemical examples of Turing patterns, in: R. Kapral, K. Showalter (Eds.), Chemical Waves and Patterns, Kluwer Academic Publishers, Dordrecht, 1995, pp. 297–322.
[18] S. Wiggins, Introduction to Applied Nonlinear Dynamical Systems and Chaos, Springer, Berlin, 1990.

[19] T.K. Callahan, E. Knobloch, Bifurcations on the FCC lattice, Phys. Rev. E 53 (1996) 3559–3562.
[20] A. De Wit, Brisure de symétrie spatiale et dynamique spatio-temporelle dans les systèmes réaction–diffusion, PhD Thesis, Brussels: Université Libre de Bruxelles, 1993.
[21] K. Staliunas, Three-dimensional Turing structures and spatial solitons in optical parametric oscillators, Phys. Rev. Lett. 81 (1998) 81–84.
[22] E.L. Thomas, D.B. Alward, D.J. Kinning, D.C. Martin, D.L. Handlin Jr., L.J. Fetters, Ordered bicontinuous double-diamond structure of star block copolymers: a new equilibrium microdomain morphology, Macromolecules 19 (1986) 2197–2202.
[23] J. Schnakenberg, Simple chemical reaction systems with limit cycle behaviour, J. Theor. Biol. 81 (1979) 389–400.
[24] J. Boissonade, E. Dulos, P. De Kepper, Turing patterns: from myth to reality, in: R. Kapral, K. Showalter (Eds.), Chemical Waves and Patterns, Kluwer Academic Publishers, Dordrecht, 1995, pp. 221–268.